THEORETICAL AND EXPERIMENTAL PRESSURE DISTRIBUTIONS FOR A 71.2° SWEPT ARROW-WING CONFIGURATION AT SUBSONIC, TRANSONIC, AND SUPERSONIC SPEEDS

Percy J. Bobbitt
NASA Langley Research Center

Marjorie E. Manro
Boeing Commercial Airplane Company

SUMMARY

A wind-tunnel test of an arrow-wing body configuration consisting of flat and twisted wings, as well as a variety of leading- and trailing-edge control-surface deflections, has been conducted at Mach numbers from 0.40 to 2.50 to provide an experimental data base for comparison with theoretical methods. Theory-to-experiment comparisons of detailed pressure distributions have been made using current state-of-the-art and newly developed attached- and separated-flow methods. The purpose of these comparisons was to delineate conditions under which these theories can provide accurate basic and incremental aeroelastic loads predictions. It was determined that current state-of-the-art linear and nonlinear attached-flow methods were adequate only at small-angle-of-attack cruise conditions. Of the several "separated-vortex" methods evaluated only the one utilizing a combination of linear source and quadratically varying doublet panels showed promise of yielding accurate loads distributions at moderate to large angles of attack. Force and moment predictions using the Polhamus suction analogy agreed well with experiments for both flat and twisted wings.

INTRODUCTION

The determination of critical design loads for various structural components of aircraft employing highly swept wings requires an examination of the loads at flight conditions involving moderate to high angles of attack. Moderate and high angles of attack in turn give rise to a flow-separation vortex at the wing leading edge. When one has to rely on theory for these loads, as is usually the case in parametric studies or for incremental aeroelastic effects, the lack of a validated analytical technique presents quite a dilemma. Inaccuracies in the predicted pressure distribution and related loads may result in an erroneous evaluation of aeroelastic effects, leading to understrength or overweight designs, performance panalties and reduced fatigue life. Aircraft stability and control estimates and control-surface-effectiveness calculations will also suffer from inaccurate loads information.

The problem of predicting aerodynamic pressure distributions on highly swept wings at moderate to high angles of attack is by no means a new one. It has received the attention of a number of theoreticians both here and abroad over the past 25 years (e.g., refs. 1 to 5) but, unfortunately, their attempts have met with only marginal success. Some relief may be forthcoming, however, in the form of methods now being developed by Boeing under contract to the Langley Research Center (ref. 6) and at Virginia Polytechnic Institute and State University (ref. 7).

At low-incidence cruise conditions the situation is much better. Attached-flow linear theories of both the lifting surface and discrete singularity type have been found to be generally adequate for aerodynamic calculations for highly swept wings. Uncertainty, however, as to the angle of attack (for a given wing geometry) at which one should cease to rely on these methods has limited their utility. In addition, the scarcity of detailed pressure data on a given configuration at both subsonic and supersonic speeds has prevented a comprehensive assessment of the unified subsonic-supersonic panel methods.

Of course, analytical methods are not the only predictive weapons aerodynamicists have at their disposal. Wind-tunnel pressure tests on a specific wing shape may be extrapolated by means of an aeroelastic solution to obtain the load distributions for other elastically deformed shapes of that wing. Methods for doing this for subsonic-transport-type wings are well developed and substantiated by flight tests. However, for highly swept wings and/or transonic flight conditions where various nonlinear phenomena become important, no satisfactory methods are available. Unless we develop reliable empirical techniques or analytical methods, such as discussed earlier, for these types of wings, the choice between extensive tunnel tests simulating a variety of flight conditions and a nonoptimum design will remain.

The primary purpose of this paper is to report on the results of a study carried out to define the ability of state-of-the-art as well as newly developed techniques to predict detailed pressures over configurations with highly swept wings. A second purpose is to describe the scope of the experimental program carried out on an arrow-wing configuration to make the present theory/experiment comparisons more comprehensive. The variety of configurational effects examined and the wide Mach number range of the tests conducted make the data obtained especially valuable for determining the efficacy of predictive techniques, present and future. Two wings were tested in the experimental program; each had the same planform and airfoil section but one was flat and the other twisted. Both were equipped with trailing-edge controls while the flat wing had leading-edge controls as well. In addition, the "basic" rounded leading edge on the flat wing could be replaced with a sharp one.

Theories evaluated in the present paper with the aid of the "arrow-wing" pressure and force data obtained in the experimental program include linear and nonlinear attached-flow methods and several separated-flow techniques. Results of calculations made using the Polhamus suction analogy (ref. 8) will also be shown even though this technique does not provide detailed pressure distributions. They are included because the method is particularly effective in predicting forces and moments and because the longitudinal load distributions

determined by this method have been used in conjunction with the Smith separated-flow method (ref. 3) in an effort to provide a better overall detailed pressure/force predictive capability.

Attempts have been made to predict not only the basic pressure distributions on a representative sample of configurations and free-stream conditions but also the incremental pressure changes due to twist. The latter is of interest since this calculation is similar to that often made to correct basic, rigid-model, wind-tunnel data for aeroleastic effects on the full-scale airplane. Incremental pressures have been evaluated by both attached- and separated-flow theories.

Results of the subsonic and transonic phase of the present program are summarized in NASA SP-347 (ref. 9) and discussed in more detail in reference 10. Some preliminary results of the supersonic phase are given in reference 11; complete results are contained in reference 12.

SYMBOLS AND ABBREVIATIONS

b	wingspan
BL	buttock line
c	local chord
$\bar{c}$	mean aerodynamic chord
c_r	root chord
C_m	pitching moment coefficient (moments about $0.25\bar{c}$)
C_N	normal force coefficient
C_n	section normal force coefficient
C_P	pressure coefficient
ΔC_P	lifting pressure coefficient
C_s	suction force coefficient
L.E.	leading edge
M	Mach number
MS	model station
s	local wing semispan

T.E.	trailing edge
x,y,z	orthogonal coordinates
α	angle of attack
γ	semiapex angle of wing
$\delta_{T.E.}$	trailing-edge control-surface deflection
ϕ	velocity potential

Subscripts x, y, and z denote differentiation.

MODELS

The wind-tunnel-model configuration chosen for the present study is shown in figure 1. It is comprised of a highly swept (71.2^{o}) wing of aspect ratio 1.65 mounted on the bottom side of a slender body. Actually two separate wings were constructed with the planform and airfoil section shown in figures 1 and 2. The only difference between the two was that one was flat, i.e., with no camber or twist, and the other was twisted (no camber). The twist distribution, which is plotted in figure 1, was taken from a supersonic cruise transport concept and modified over the inboard third to facilitate model construction.

Both wings were equipped with 25-percent-chord trailing-edge control surfaces which were split at the 57-percent semispan station to permit partial as well as full span streamwise deflections of 0^{o}, $\pm 4.1^{o}$, $\pm 8.3^{o}$, $\pm 17.7^{o}$, and $\pm 30.2^{o}$. In addition, the flat wing was provided with removable leading-edge segments that extended over 15 percent of the streamwise chord. These segments permitted testing of the leading-edge segment in two drooped positions, 5.1^{o} and 12.8^{o}, as well as undeflected. In order to investigate the effect of leading-edge shape, a second segment was constructed with a sharp leading edge. A sketch of the basic rounded leading edge with the sharp leading edge superimposed is given in figure 1.

The 217 pressure orifices on the wing were equally divided into 7 streamwise sections on the left wing. Pressure taps were located on both the top and bottom surfaces at the chordwise locations shown in figure 2. The body orifices were arranged in 5 streamwise rows of 15 orifices each. An additional 8 orifices in the area of the wing-body junction made a total of 83 orifices on the left side of the body.

The model was constructed of steel to minimize aeroelastic deflections. To ensure close control of the model dimensions, a computerized lofting program was used to provide data for machining the model components using numerically controlled operations.

WIND-TUNNEL TESTS

The model was tested in the Boeing Transonic Wind Tunnel (BTWT) and in the supersonic 9- by 7-foot leg of the NASA Ames Unitary Wind Tunnel. The former is a continuous-flow, closed-circuit, atmospheric facility with a 12.5-percent porosity test section measuring 8 by 12 by 14.5 feet; the latter is a continuous-flow, closed-circuit, variable-density facility with a test section measuring 7 by 9 by 18 feet. Photographs of the model in the Boeing and NASA Ames tunnels are given in figures 3 and 4. Seven Mach numbers from 0.40 to 1.11 were tested in the BTWT, with angle of attack varying from -8^{o} to $+16^{o}$. In the Ames facility, data were obtained primarily at Mach numbers of 1.7, 2.1, and 2.5. A few selected tests were run at a Mach number of 1.5 to provide better continuity of pressure as a function of Mach number. However, at this Mach number the shock from the nose of the model reflected off the wall back across the wing tip and only those pressures forward of the shock are valid. The major configurations tested are shown in tables I and II.

THEORETICAL METHODS

Theoretical calculations utilized in this paper are based on inviscid theories for both attached and detached flows. Results from three attached-flow theories are discussed: one uses the linear, subsonic/supersonic, constant-pressure-panel formulation, the second uses a panel solution of the exact incompressible-flow equation satisfying the exact boundary condition on the configuration surface, and the third solves the exact, nonlinear, full-potential equation using a finite difference technique.

Four separated-flow methods are examined; the first is the conical flow method of J. H. B. Smith outlined in reference 3. The second method is due to E. C. Polhamus and is widely known as the leading-edge suction analogy. The third method (more aptly termed a technique) is one which combines the Polhamus suction analogy with the Smith method. The last method to be examined is based on distributions of quadratically varying doublet and linearly varying source panels. Since this approach is still under development and only preliminary results are available, a final judgment on the accuracy of the method is not possible. However, it does have the ability to treat a wide variety of wing-body configurations while the older separated-flow methods can handle only simple wing geometries.

Because of the strong influence of the leading-edge vortex for angles of attack greater than a few degrees, attached-flow theories can be expected to yield good agreement only at low angles of attack. Detached-flow theories, on the other hand, should be able to do a good job of predicting loading trends at high angles of attack although they cannot now handle as geometrically complex configurations as the more mature attached-flow methods. Additional details of the analytical methods are discussed briefly in the next section.

Attached-Flow Theories

One of the most popular linear panel techniques in use today is the unified, subsonic/supersonic constant-pressure-panel method developed by Woodward (refs. 13 and 14). In the present study a slightly improved version of the original Woodward program contained in the FLEXSTAB system of programs (see refs. 15 to 17) has been chosen for evaluation. It should be noted that the FLEXSTAB aerodynamic module has been employed as the basic loads tool for another SCAR study (ref. 18) and is utilized in the FLEXSTAB system to evaluate the static and dynamic stability, the inertial and aerodynamic loading, and the resulting aeroelastic deformations of aircraft configurations.

The paneling scheme utilized for the research arrow wing of the present study is depicted in figure 5. Note that the panels are of nearly equal width, their leading and trailing edges are at constant percent chord, and they are more concentrated near the wing leading edge and at the flap hingelines. In addition, the edges of the panels were chosen to coincide with the control-surface hingelines and breaklines.

In the Woodward/FLEXSTAB panel method, line sources and doublets are distributed along the longitudinal axis of the body to simulate its thickness and lifting effects. Similarly, source and vortex panels are placed in the plane of the wing to simulate its thickness and lifting effects. To account for the interference effects between the wing and body, constant-pressure vortex panels are placed on a shell around the body. This "interference" shell serves to cancel the normal velocity components on the body induced by the wing. At subsonic Mach numbers and the high supersonic Mach numbers, 50 line singularities, 168 interference panels, and 160 wing panels were used to represent the configuration. For the very low supersonic Mach numbers (1.05 and 1.11), the number of interference panels had to be greatly increased (to 330) to overcome instabilities associated with the solution.

The second attached-flow method to be evaluated is that of Rubbert and Saaris (refs. 19 and 20) for the numerical solution of the exact incompressible potential-flow equation (Laplace's equation), with compressibility effects incorporated via the Gothert rule. In contrast to FLEXSTAB, the Rubbert-Saaris (hereafter referred to as TEA-230) solution satisfies the exact boundary conditions rather than approximate linear ones.

Figure 6 shows a typical paneling scheme used for the TEA-230 representation of the arrow-wing body model. The source panels are placed on the configuration surface; consequently, new paneling was required for each configuration. Linearly varying internal and trailing vortex panel networks are also used but not shown. (See ref. 10.) The number of source and vortex panels was different for each configuration but in every case more than 800 source and 280 vortex panels were used.

The third attached-flow method whose ability to predict arrow-wing pressures is to be determined is that of A. Jameson and D. A. Caughey.

This method, which is still under development, employs a finite difference technique to solve the full nonlinear potential equation for three-dimensional flow. Satisfaction of the exact boundary conditions is facilitated by the use of a sheared parabolic coordinate system in which the airfoil surface is coincident with a coordinate line. (See fig. 7.) The grid is stretched in all three coordinate directions to minimize the number of total grid points. In the calculations presented in the present paper approximately 60 grid points are employed on the top and bottom of the airfoil section at the wing root (total of 120) and 15 on the top and bottom of the tip section. With longitudinal grid networks located at each of 21 spanwise stations on the wing, the resolution obtained is more than twice that of the TEA-230 method. While the method has only been applied to plain wings (no body), there is almost no limit to the type of wing geometries that it can treat.

Detached-Flow Theories

A number of methods are available which have the capability of accounting for the leading-edge separated vortex. Many of these make the assumption that the flow is conical and, as a consequence, are able to reduce the three-dimensional problem to a two-dimensional one. Wing planforms that conical methods are able to treat are generally limited to deltas though an extension to cranked deltas has been effected (ref. 5). The trailing-edge Kutta condition is not satisfied in these programs.

One of the best known of the "conical" separated-flow programs is that developed by J. H. B. Smith of the RAE (ref. 3). This approach was published in 1966 and is an improved version of the well-known Mangler-Smith method of 1957. Solutions obtained with this method satisfy the leading-edge Kutta condition and that of pressure continuity across the vortex sheet. In addition, the vortex sheet is constrained to be a stream surface of the three-dimensional flow. The solution technique utilizes a conformal transformation which in effect opens the wing (positioned on the horizontal axis) into a circle and then squeezes it into a vertical slit. The wing tips map onto the origin of the transformed plane and the midpoints of the upper and lower surfaces are located on the vertical axis equidistant from the origin. The outer vortex sheet in the transformed plane is approximated by a series of linear segments, typically 20 to 40 in number, which are joined by a cut to a potential vortex core. An iterative technique is used to determine the shape of the vortex sheet, the strength of the sheet segments, and the vortex core.

As noted in the Introduction, results from the Polhamus suction analogy would be presented even though it does not produce detailed pressures. It does, however, predict longitudinal load distributions and it is capable of doing an excellent job on the lift and pitching moment of arbitrary wing geometries. Details of this method were first published in 1966 in reference 8; improvements in the "analogy" since that time have greatly increased its capabilities. (See ref. 21.) In a subsequent paragraph, two simple procedures for using the suction analogy longitudinal load distribution along

with the Smith separated-vortex method to obtain "improved" pressure distributions will be described.

The basic features of the suction analogy are depicted in figure 8. The bottom left-hand side of the figure depicts the attached-flow situation where linear theory predicts a square singularity in the pressure at the leading edge. This singularity in turn produces a suction force in the plane of the wing. In practice the flow at moderate angles of attack becomes like that depicted on the right-hand panel of the wing in figure 8. The flow separates off the leading edge, a vortex forms above the wing, and the flow reattaches inboard of the leading edge. The suction analogy assumes that the force required to make the flow over the vortex attach on the upper surface is the same as the leading-edge suction force which was lost when the flow separated.

Suction force calculations carried out for the present paper were determined using pressure distributions calculated by the FLEXSTAB aerodynamic module discussed earlier. These were added to the potential-flow lift modified for large angles of attack to obtain the total lift.

Since the suction analogy is known to provide good estimates of the force and moment of slender wings one would expect that the longitudinal load distributions determined by the method would also be in good agreement with experiment. One advantage that the suction analogy has over conical separated-vortex methods in producing accurate longitudinal load distributions is that it is based on potential-flow methods which satisfy the trailing-edge Kutta condition where appropriate. While the suction analogy can produce reasonably accurate longitudinal load distributions it is incapable of predicting detailed pressures. On the other hand, the conical separated-flow methods yield pressure distributions with the right character but not always the right magnitude. These two facts suggest the possibility that a semi-empirical method combining both of these approaches would do a better overall job. Two ways of expediting this marriage have been investigated. The first would simply take the local Smith spanwise pressure distributions and multiply them by the ratio of the local normal force obtained from the suction analogy by that obtained by the Smith method; i.e., the integration of the spanwise pressure distribution. The second empiricism would be to calculate the local spanwise pressure distributions with the Smith method using values of the parameter "a" = ($\tan \alpha / \tan \gamma$) which produces the same local normal force as the suction analogy. This can be done rather easily by working backward from the empirical equation given in reference 3 for the <u>total</u> normal force coefficient.

A new method for the prediction of wing pressures including the effect of the leading-edge spiral vortex is now being developed under contract to NASA Langley Research Center (refs. 6 and 22). This method is capable of predicting forces, moments, and detailed surface pressures on wings of arbitrary planform, thickness, camber, and twist distributions mounted on a fuselage. The wing geometry is arbitrary in the sense that leading and trailing edges may be swept as well as curved or kinked.

The governing equation is the linear potential flow equation with nonlinear boundary conditions which require that the flow be parallel to the wing surface and that the free vortex sheet, springing from the leading and trailing edges, be alined with the local flow and support no pressure jump. The Kutta condition is imposed and satisfied along all wing edges. This problem is solved numerically by an aerodynamic panel method. The configuration is represented by quadrilateral panels on all surfaces with quadratically varying doublet and linear source singularities distributed on them. The vortex core is modeled as a simple line vortex that receives vorticity from the free sheet through a connecting kinematic sheet. The set of nonlinear equations is solved by an iterative procedure, starting with an assumed initial geometry.

Figure 9 shows the type of paneling arrangement used on the wing. Note that the leading and trailing edges are extended for the sake of simplicity to a point rather than chopped off to form a finite tip. This should have only a trivial effect on the answers obtained. The fuselage was not a part of the current model; instead, the wing external to the body was moved inboard to obtain a more realistic model of the wing alone. Results from two different paneling densities are used in the present paper. For the detailed comparison of the basic flat wing, pressure distribution a total of 212 panels was used: 63 panels to describe the wing, 108 panels to describe the rolled-up vortex, and 41 panels to describe the wake. In making a prediction of the incremental load due to twist a total of 142 panels was used with 49 on the wing.

LEADING-EDGE VORTEX CHARACTERISTICS

The large effect of the separated vortex on the flow field above the wing has been mentioned previously but only in general terms. It is helpful in trying to evaluate theory/experiment comparisons to have in mind a good picture of how the vortex develops and how it is affected by changes in the free-stream conditions or wing geometry. Some of this knowledge can be obtained by looking at upper-surface isobar plots. A large number of these plots has been generated; only a representative few will be shown here to emphasize the major effects.

Figure 10 shows formation and development of the leading-edge vortex on the basic rounded-leading-edge, flat wing at a Mach number of 0.40. At 2^{o} angle of attack the isobars have the configuration typical of attached flow. Even at 4^{o} the isobars have a "potential" look except perhaps near the tip where there is some evidence of vortex formation. The isobar plot for 8^{o} angle of attack shows a well-developed vortex that dominates the flow over the outboard third of the wing. For the $\alpha = 16^{o}$ case the vortex is clearly affecting the flow over the entire wing.

The development of the leading-edge vortex with increasing angle of attack is influenced by the sharpness of the leading edge, wing twist, and wing camber for a given wing planform. Tests on a cambered arrow wing have

not yet been carried out but data are available to yield some idea of the effect of leading-edge radius and wing twist. The first of these influences can be seen by comparing the isobars of figure 10 with those of figure 11, which are for the sharp-leading-edge flat wing. It is evident from figure 11 that the vortex develops much more rapidly for the sharp leading-edge wing than for the round. The sharp-leading-edge vortex for 4^{o} angle of attack is almost as well developed as the round-leading-edge one is at 8^{o}. This contrast tends to diminish as Mach number and angle of attack are increased. For instance, at 16^{o} angle of attack the difference between the sharp- and rounded-leading-edge isobar configurations is negligible.

A comparison of figure 12 with figure 10 gives one a good idea of the effect of twist on vortex formation. An angle of attack of nearly 8^{o} is required to produce the same kind of isobar configuration as was evident at 4^{o} on the flat wing. Since the local angles of attack for the twisted wing are less than those of the flat wing this type of behavior is not surprising.

Finally, the effect of Mach number on vortex movement can be seen by comparing the isobar plots of figure 13 for an $M = 2.5$ with those of figure 10 which were for $M = 0.40$. At $M = 2.5$ the vortex appears to form at only a few degrees angle of attack but is not as concentrated as at the subsonic Mach number. For $\alpha = 8^{o}$ the vortex appears to be fairly well formed and much further inboard than it was at $M = 0.40$. Not noted on the isobar plots, but significant, is the fact that the increment in pressure between isobars on the $M = 2.5$ plot is a factor of 5 to 10 less than on the $M = 0.40$ plot. While there is clearly a vortex type flow at $M = 2.5$, it is very much weaker than that at $M = 0.40$.

TEST-THEORY COMPARISONS

The real value of any aerodynamic theory lies in its ability to accurately predict flight or wind-tunnel results. Consequently, the predictive methods that designers normally use, or that the theoreticians have just developed and hope will find acceptance, must be evaluated through comparisons with experiment. Of course the configurations and free-stream conditions used for the comparisons should be as similar as possible to those which one eventually expects to apply the theory. With this in mind, and recognizing the limited amount of detailed pressure data available for arrow-wing configurations which spans both subsonic and supersonic speed regimes, the present experimental program and associated theoretical-methods evaluation were undertaken. Subsequent sections will describe a number of theory/experiment comparisons made in effecting an evaluation of some of our state-of-the-art and newly developed methods.

Attached-Flow Methods

Before examining theory/experiment pressure-distributions correlation it is instructive to take a look at the ability of the linear attached theories

to predict gross aerodynamic quantities. A comparison is shown in figures 14 and 15 of experimental and theoretical normal force and pitching moment coefficients over the complete Mach number range for the FLEXSTAB program and at subsonic speeds for the TEA-230 method. The calculations are in good agreement with experiment for all Mach numbers at low angles of attack. However, at moderate angles the TEA-230 method underpredicts the data; the FLEXSTAB methods continue to agree quite well. This agreement is fortuitous, as will be seen in the subsequent discussion, and points up once again the well-known fact that detailed pressure distributions are required to determine the adequacy of theoretical methods for predicting load distributions on wings.

Chordwise distributions of experimental and theoretical surface pressure on the flat-wing configuration are shown in figures 16 to 23 for four Mach numbers. Data are presented for three spanwise stations, 20, 50, and 80 percent of the semispan, and at angles of attack of 4° and 12°. At the low angle of attack, generally good agreement with experimental results was obtained by the use of either attached-flow theory. However, the lack of agreement of the upper-surface pressures at the most outboard station at Mach numbers of 0.85 and 1.05 is due to the start of vortex formation. At $M = 1.7$ the midspan and outboard sections are affected by the vortex. No significant degradation of the agreement due to separation is evident for a Mach number of 2.5. The TEA-230 predictions are somewhat better near the leading edge than the FLEXSTAB results, which exhibit the typical linear theory leading-edge singularity.

At 12° angle of attack good agreement of the predictions with the experimental data is obtained only at the most inboard wing section ($2y/b = 0.20$) for $M = 0.85$ and 1.05. (See figs. 17 and 19.) At the two outboard stations, neither the FLEXSTAB nor the TEA-230 results compare well with experimental data. The distributions for $M = 1.7$ (fig. 21) indicate a substantial effect of the vortex at the midspan station, but because the vortex crosses the trailing edge just beyond this station the theory/experiment agreement is much better in the outboard region of the wing. Isobar plots indicate that at $M = 2.50$ the vortex crosses the trailing edge inboard of the midspan station; consequently, the theory in figure 23 does a better job at the outboard stations than it did at lower Mach numbers. One final point of interest with respect to these chordwise pressure distributions is the diminishing effect of the leading-edge vortex as Mach number increases from 1.05 to 2.50.

The spanwise load distributions shown in figure 24 demonstrate the same points made earlier with respect to the chord load distributions. The agreement is best at small angles of attack and near the wing root. At high angles of attack, the theory generally underpredicts the load level over the inboard half of the wing and overpredicts it outboard. For $M = 2.5$ the lack of agreement near the wing tip for high angles cannot be attributed to the close proximity of a spiral vortex. The flow is either separated over the whole chord, giving rise to the near constant pressure, or, because the pressures are approaching the vacuum level, they cannot go any lower.

Application of the Jameson-Caughey transonic wing code to the research arrow wing yields the results depicted on figures 25 to 27. Calculations are

shown for Mach numbers of 0.85, 0.95, and 1.05 at three spanwise stations and for 4^{o} angle of attack. The Mach 1.05 calculation is particularly noteworthy since most transonic wing codes are limited to subsonic speeds ($M < 1$) by virtue of the type of differencing schemes used. The Jameson-Caughey method is able to obtain accurate theoretical results because it employs the so-called Jameson "rotated" difference scheme which takes proper account of the zone of dependence in the supersonic regions of the flow. (See ref. 23.)

Comparisons of theory and experiment at $M = 0.85$, figure 25, show excellent agreement everywhere except close to the leading edge on the upper side of the most outboard station. This discrepancy, as noted earlier, is caused by the formation of the leading-edge vortex. Numerical results obtained using the Jameson-Caughey program are very similar to those obtained using the TEA-230. (See fig. 16.) Correlations at $M = 0.95$, shown in figure 26, are also quite good but the vortex formation at the tip has a larger effect on the pressure distribution at this Mach number and the upper surface agreement is correspondingly degraded.

Finally at $M = 1.05$ (see fig. 27) there seems to be an upward shift of the experimental data relative to the theory. This is particularly noticeable over the rear half of the distributions for $2y/b = 0.2$ and 0.5. It is not clear whether this is due to the effect of the body (not accounted for in the theory), the effect of a reflected shock from the wall, or a viscous effect.

Detached-Flow Theories

As indicated in the section on theoretical methods the leading-edge suction analogy was adapted for use with the FLEXSTAB aerodynamic module for the calculation of lift, pitching moment, and longitudinal load distribution. Four arrow-wing configurations were analyzed - the flat wing, the twisted wing, and the flat wing with 5.1^{o} and 12.8^{o} leading-edge control-surface deflection. (See ref. 10.) Only results from the first two of these configurations will be discussed here.

Comparisons of the calculated total lift, pitching moment, and longitudinal load distribution for the flat and twisted wings at a Mach number of 0.85 are given in figures 28 to 31. The potential solution by itself underpredicts the experimental results; adding the vortex lift yields a total which overpredicts experiment. The fact that the theory assumes a flat sharp-edged wing would lead one to expect better agreement with the sharp-leading-edge data in figure 28 than with the round edge. This seems to be the case, at least for the lift.

A recent improvement to the suction analogy method, termed the augmented vortex-lift concept, when applied to wings with swept-back trailing edges results in a negative lift and moment increment. Calculations for the arrow-wing increments were made by John E. Lamar of NASA Langley Research Center and are labeled on figure 28 as the augmented vortex lift and augmented vortex increment. The prediction of total lift is clearly improved. To obtain the effect on pitching moment, the augmented vortex lift is placed at

the two-thirds semispan station on the trailing edge. As in the lift case the pitching moment prediction is improved by the augmented vortex increment.

Whereas the augmented vortex concept does not provide for a method of predicting the associated reductions in the longitudinal load distribution, it does indicate that the loss would occur in the region aft of the apex of the trailing edge. This seems to be confirmed by the overprediction of the experimental load aft of the trailing edge shown in figure 30.

Lift and moment curves for the twisted wing are plotted in figure 29. The agreement of the vortex plus potential lift and moment with experiment are about the same as for the flat wing. Indeed the curves are almost identical; twist primarily causes a shift of two to three degrees in the zero-lift and zero-moment angles of attack. On this basis, the augmented vortex increments for the twisted wing should be nearly the same as for the flat wing; they would just be added to the lift and moment at an angle of attack 2° greater.

Theoretical predictions of the longitudinal load distributions for the flat and twisted wing exceed the experimental values over the whole length of the wing. Generally the differences are not large so the agreement may be termed fair to good.

The next detached-flow method to be compared with experiment is that due to J. H. B. Smith of the Royal Aircraft Establishment. This method yields detailed pressures but only for incompressible flow. Another limitation to the application of the Smith method derives from the assumption of conical flow; i.e., the pressures beyond the trailing-edge apex cannot be determined. Consequently, comparisons of the theoretical and experimental spanwise variations of the lifting pressure have been made only for longitudinal locations up to 93 percent of the root chord.

Figure 32 shows results from the Smith method compared to interpolated sharp-edged wing experimental data ($M = 0.40$) for x/c_r values of 0.55, 0.74, and 0.93 and an angle of attack of 12°. At $x/c_r = 0.55$, the Smith method agrees fairly well inboard but peaks at a value almost twice that of the experimental maximum. As one moves toward the trailing edge, the agreement inboard deteriorates to where at $x/c_r = 0.93$ the theoretical level is almost twice the experimental. This is probably due to the fact that the Smith method does not satisfy the Kutta condition.

The large differences in the peak pressures outboard indicate that the theoretical vortex strength is too large or the vortex is too close to the surface. Experimental data summarized in reference 3 indicate that, for a $\tan \alpha/\tan \gamma$ ratio less than 1.0 (the arrow wing for $\alpha = 12^{\circ}$ yields a value for $\tan \alpha/\tan \gamma$ of approximately 0.6), the vortex will generally be higher and further inboard than the theoretical location. Reference 3 also indicates that for $\tan \alpha/\tan \gamma$ ratio on the order of 1.0 or larger the position of the vortex is better predicted and the maximum pressures are in much better agreement with experiment.

A second calculation has been made using the Smith method by constraining the spanwise integration of pressure distribution; i.e., the local value of the longitudinal load, to have the same value as that given by the suction analogy. As noted in the section on theoretical methods there are two ways of doing this. The calculations shown on figure 32 (modified Smith method) are for the technique wherein the value of $\tan\alpha/\tan\gamma$ is used which gives the same value of the longitudinal load as the suction analogy. A comparison of this modified Smith method with experiment and the original Smith method shows some improvement inboard of the midspan stations but no significant improvement outboard. The second empiricism suggested for the Smith method, whereby the pressures are simply multiplied by the ratio of the suction analogy and Smith method longitudinal loads, provided no better agreement than that shown in figure 32.

The last detached-flow method to be evaluated with the aid of arrow-wing pressure data is an improved version of the panel method detailed by Weber et al. in reference 6. (See ref. 22.) A brief description of its features, including the paneling arrangement, was given in the theoretical methods section. Panel-method calculations for $M = 0$ have been made for the same longitudinal location and angle of attack as those shown in figure 32 for the "Smith" method. Figure 33 compares these results with the sharp-edged wing data for $M = 0.40$. (Note the ordinate scale in fig. 33 is one-half that of fig. 32.) It is quite clear from figure 33 that the separated-flow panel method correlates with experiment much better than the Smith method, doing a good job on the level of the inboard pressures as well as the outboard pressure peak. Spanwise distributions of pressure for locations aft of the trailing-edge apex (not shown in fig. 33) remain quite good although the theoretical pressure peaks exceed the experimental ones. (See ref. 11.)

SIMULATED AEROELASTIC CALCULATIONS

Aside from parametric studies, theoretical methods are used mainly to correct experimental data from a rigid wind-tunnel model for the effects of the elastic deformation of the aircraft structure under load. Examples of this procedure are shown in figures 34 and 35 for Mach 0.85 and 2.1 at an angle of attack of 8°. Here experimental data for the flat wing are taken as representative of a typical rigid-model tunnel test. A theoretical increment calculated for the known twist of the model (supposed elastic deformation) using the FLEXSTAB program is added to obtain the predicted distribution. This result is compared with the twisted-wing data at the same angle of attack (deformed airframe). Three spanwise locations are shown; the section at $2y/b = 0.35$ is typical of the other inboard stations. The error in predicting the pressure distribution is small at the inboard stations, primarily because the relative twist in this region is small. However, there are significant differences at the midspan and outboard stations between the experimental flat-wing data theoretically corrected for twist and the experimental twisted-wing data. This is because the linear FLEXSTAB program does not account for the nonlinear vortex effects.

Since the linear attached-flow methods do not do an adequate job of providing aeroelastic corrections of highly swept wings, at least for the effect of twist, it is of interest to determine if the separated-flow panel program of reference 22 can do any better. Figure 36 shows the results of a crude first attempt. Spanwise rather than chordwise variations of pressure are presented due to the paneling arrangement. (See fig. 7.) It should also be noted that wing thickness and the fuselage were not accounted for in the panel model used and only 49 panels were employed on the wing (7 rows of panels with 7 panels each).

Calculations have been carried out for the flat and twisted wing at $M = 0.40$ and an angle of attack of 12°. As in the calculations for figures 34 and 35 the increment between these two theoretical results has been added to the flat-plate experimental data. The simulated aeroelastic prediction for the twisted wing is the solid line and should be judged by the square symbols for the twisted-wing experimental results. In the outboard region at the $x/c_r = 0.435$ station, where the experimental differences are large, the simulated aeroelastic prediction does not agree with the twisted wing data. At $x/c_r = 0.91$ the agreement is quite good with the largest discrepancy occurring around the 75-percent semispan station. Agreement between the prediction and the twisted-wing data deteriorates considerably in moving from the $x/c_r = 0.91$ station to $x/c_r = 1.26$. Theory says that the increment is negative everywhere, whereas experimentally there are both positive and negative increments. Overall one would have to say that the separated-vortex panel program did not do much better than the linear attached-flow panel method in predicting the "aeroelastic" increment. However, it should be remembered that the paneling scheme was very crude (49 panels on the wing) and the fuselage and wing thickness were not accounted for. Certainly the 63-panel calculation for the flat wing shown in figure 33 offers some hope that when the full capability of the program now being developed can be utilized more accurate incremental predictions will result.

CONTROL SURFACE EFFECTS

The experimental program carried out on the arrow-wing model included a number of tests with the leading and trailing edges deflected. (See Tables I and II.) As in the case of the basic flat and twisted wings, theoretical calculations were carried out for the deflected-control configurations using the FLEXSTAB and TEA-230 programs. A sample of these calculations is shown in figure 37 which depicts the change with Mach number of the chordwise distribution of pressure for a trailing-edge, control-surface deflection of 8.3° and the wing at zero angle of attack. The station $2y/b = 0.65$ is used in this figure since the agreement between theory and experiment is typical of that obtained at other spanwise stations. It is apparent from figure 37 that the prediction of the pressures at the leading edge and at the hingeline are much better with the TEA-230 method (only $M = 0.40$ calculation shown) than with FLEXSTAB. FLEXSTAB overpredicts the pressures on the control surface at all Mach numbers shown, although at this angle of attack the distribution

forward of the hingeline is quite good except at the leading edge. For higher deflection angles, i.e., 17.7 and 30.2°, the flow separates on the bottom side of the flap and the agreement becomes worse. Also as the flap angle is increased at subsonic speeds the circulation induced by the flap causes a leading-edge vortex to form, further impairing the agreement of theory and experiment near the tip. Similarly, when the wing is at an angle of attack sufficient to cause the formation of a leading-edge vortex the effectiveness of the outboard part of the trailing-edge control is greatly reduced. (See ref. 11.)

CONCLUDING REMARKS

It has been shown that the attached-potential-flow methods can yield good agreement with experimental data for a highly swept, arrow-wing configuration only at low angles of attack such as one encounters at cruise conditions (load factor one). At critical structural and control design conditions, which usually involve moderate to large angles of attack and/or large control-surface deflections, the attached-flow theories are inadequate. Attempts to introduce empirical corrections using attached- and detached-flow methods have been unsatisfactory.

Calculations for four separated-flow methods were compared to theory. The Polhamus suction analogy, which does not provide predictions of the detailed pressures, showed generally good agreement for the lift, moment and longitudinal load predictions for both flat and twisted wings. Detailed pressure distributions calculated using the Smith conical flow method and two slightly modified versions of the Smith method did not agree well with experiment particularly in the vicinity of the vortex. A new detached-flow method which uses linearly varying source and quadratically varying doublet panels showed the best agreement with experimental pressure data for the basic flat-wing configuration. Further development of this type of analysis technique is mandatory if we are to be successful in predicting the pressures on wings with a separated leading-edge vortex.

The prediction of control-surface-induced and direct loads was more accurately done by the TEA-230 program which satisfies the exact boundary conditions of the wing and control surface than by the FLEXSTAB program which uses only planar boundary conditions. For high flap deflections separated flow at the hinge line degraded the theory/experiment correlation. At large flap deflections and/or angles of attack greater than 4° a leading-edge vortex existed which greatly reduced the effectiveness of the outboard half of the trailing-edge vortex.

REFERENCES

1. Brown, Clinton E.; and Michael, William H., Jr.: On Slender Delta Wings With Leading-Edge Separation. NACA TN 3430, 1955.

2. Mangler, K. W.; and Smith, J. H. B.: A Theory of Flow Past a Slender Delta Wing With Leading Edge Separation. Proc. Roy. Soc. (London), ser. A. vol. 251, no. 1265, May 26, 1959, pp. 200-217.

3. Smith, J. H. B.: Improved Calculations of Leading-Edge Separation From Slender Delta Wings. Tech. Rep. No. 66070, Brit. R.A.E., Mar. 1966.

4. Legendre, R.: Nappes de tourbillons deferlant des bords d'attaque des ailes en delta (in English). Presented to I.U.T.A.M. Symposium on Concentrated Vortex Motions, Ann Arbor, July 1964. Prog. in Aeron. Sci. (ed Kuchemann et al.) 7, Pergamon Press, Oxford, 1966.

5. Wei, M. H. Y.; Levinsky, E. S.; and Su, F. Y.: Nonconical Theory of Flow Past Slender Wing-Bodies With Leading-Edge Separation. NASA CR 73446, 1969.

6. Weber, James A.; Brune, Guenter W.; Johnson, Forrester T.; Lu, Paul; and Rubbert, Paul E.: Three-Dimensional Solution of Flows Over Wings With Leading Edge Vortex Separation. Printed in Aerodynamic Analyses Requiring Advanced Computers. NASA SP-347, pp. 1013-1032, 1975.

7. Kandil, O. A.; Mook, D. T.; and Nayfeh, A. H.: Nonlinear Prediction of the Aerodynamic Loads on Lifting Surfaces. AIAA Paper No. 74-503, June 1974. Also J. of Airc., vol. 13, no. 1, Jan 1976, pp. 22-28.

8. Polhamus, E. C.: A Concept of the Vortex Lift of Sharp-Edge Delta Wings Based on a Leading-Edge-Suction Analogy. NASA TN D-3767, 1966.

9. Manro, Majorie E.; Tinco, Edward N.; Bobbitt, Percy J.; and Rogers, John T.: Comparison of Theoretical and Experimental Pressure Distributions on an Arrow-Wing Configuration at Transonic Speed. Printed in Aerodynamic Analyses Requiring Advanced Computers. NASA SP-347, pp. 1141-1188, 1975.

10. Manro, Marjorie E.; Manning, Kenneth J. R.; Hallstaff, Thomas H.; and Rogers, John T.: Transonic Pressure Measurements and Comparison of Theory to Experiment for an Arrow-Wing Configuration. Summary Report, NASA CR-2610, 1975.

11. Manro, M. E.; Bobbitt, P. J.; and Rogers, J. T.: Comparisons of Theoretical and Experimental Pressure Distributions on an Arrow-Wing Configuration at Subsonic, Transonic and Supersonic Speeds. AGARD Conference Preprint No. 204 on Prediction of Aerodynamic Loading, Sept. 1976.

12. Manro, M. E.: Supersonic Pressure Measurements and Comparison of Theory to Experiment for an Arrow-Wing Configuration. NASA CR-145046, 1976.

13. Woodward, F. A.; Tinoco, E. N.; and Larsen, J. W.: Analysis and Design of Supersonic Wing-Body Combinations, Including Flow Properties in the Near Field. Part 1 - Theory and Application. NASA CR-73106, 1967.

14. Woodward, F. A.: Analysis and Design of Wing-Body Combinations at Subsonic and Supersonic Speeds. J. of Airc., vol. 5, no. 6, Nov.-Dec. 1968, pp. 528-534.

15. Tinoco, E. N.; and Mercer, J. E.: FLEXSTAB - A Summary of the Functions and Capabilities of the NASA Flexible Airplane Analysis Computer System. NASA CR-2564, Oct. 1974.

16. Dusto, A. R., et al.: A Method for Predicting the Stability Characteristics of an Elastic Airplane. Volume 1, FLEXSTAB Theoretical Manual. NASA CR-114712, 1974.

17. Perkin, Brian R.; and Erickson, Larry L.: FLEXSTAB - A Computer Program for the Prediction of Loads and Stability and Control of Flexible Aircraft. Proceedings of the SCAR Conference, NASA CP-001, 1977. (Paper no. 12 of this compilation.)

18. Turner, M. J.; and Hoy, J. M.: Titanium and Advanced Composite Structures for a Supersonic Cruise Arrow Wing Configuration. Proceedings of the SCAR Conference, NASA CP-001, 1977. (Paper no. 28 of this compilation.)

19. Rubbert, P. E.; Saaris, G. R.; Scholey, M. B.; Standen, N. M.; and Wallace, R. E.: A General Method for Determining the Aerodynamic Characteristics of Fan-in-Wing Configurations. Volume I, Theory and Application. USAAVLABS Technical Report 67-61A, 1967.

20. Rubbert, P. E.; and Saaris, G. R.: Review and Evaluation of a Three-Dimensional Lifting Potential Flow Analysis Method for Arbitrary Configurations. AIAA Paper No. 72-188, 1972.

21. Lamar, John E.: Some Recent Applications of the Suction Analogy to Vortex-Lift Estimates. Printed in Aerodynamic Analyses Requiring Advanced Computers. NASA SP-347, pp. 985-1912, 1975.

22. Gloss, Blair B.; and Johnson, Forrester, T.: Development of an Aerodynamic Theory Capable of Predicting Surface Loads on Slender Wings With Vortex Flow. Proceedings of the SCAR Conference, NASA CP-001, 1977. (Paper no. 3 of this compilation.)

23. South, Jerry C., Jr.; and Jameson, Antony: Relaxation Solutions for Inviscid Axisymmetric Transonic Flow Over Blunt or Pointed Bodies. AIAA Computational Fluid Dynamics Conference. Palm Springs, Calif., July 1973, pp. 8-17.

TABLE I.- SUMMARY OF CONDITIONS TESTED IN BOEING TRANSONIC WIND TUNNEL

WING	TRAILING EDGE	LEADING-EDGE DEFLECTION, degrees	TRAILING-EDGE DEFLECTION, degrees
ROUNDED-LEADING-EDGE FLAT WING	FLAT	0	0, ± 4.1, ± 8.3, ± 17.7, ± 30.2
			PARTIAL SPAN ± 8.3, + 17.7
		PARTIAL SPAN 5.1	PARTIAL SPAN ± 8.3, ± 17.7
		5.1, 12.8	0, + 4.1, ± 8.3, ± 17.7
	TWISTED	0	0, + 4.1, ± 8.3, ± 17.7
SHARP-LEADING-EDGE FLAT WING	FLAT	0	0
ROUNDED-LEADING-EDGE TWISTED WING	TWISTED	0	0, + 4.1, ± 8.3, ± 17.7, + 30.2

MACH NUMBERS: 0.40, 0.70, 0.85, 0.95, 1.00, 1.05, 1.11
ANGLE OF ATTACK: -8^0 TO $+16^0$ (2^0 INCREMENTS)

TABLE II.- SUMMARY OF CONDITIONS TESTED IN NASA AMES UNITARY WIND TUNNEL

WING	TRAILING EDGE	LEADING-EDGE DEFLECTION, degrees	TRAILING-EDGE DEFLECTION, degrees
ROUNDED-LEADING-EDGE FLAT WING	FLAT	0	0, ± 4.1, + 8.3
			PARTIAL SPAN + 4.1, + 8.3
		5.1	0
SHARP-LEADING-EDGE FLAT WING	FLAT	0	0
		5.1	0
ROUNDED-LEADING-EDGE TWISTED WING	TWISTED	0	0, + 8.3

MACH NUMBERS: 1.70, 2.10, 2.50
ANGLE OF ATTACK: -8^0 TO $+14^0$ (2^0 INCREMENTS) + 15^0

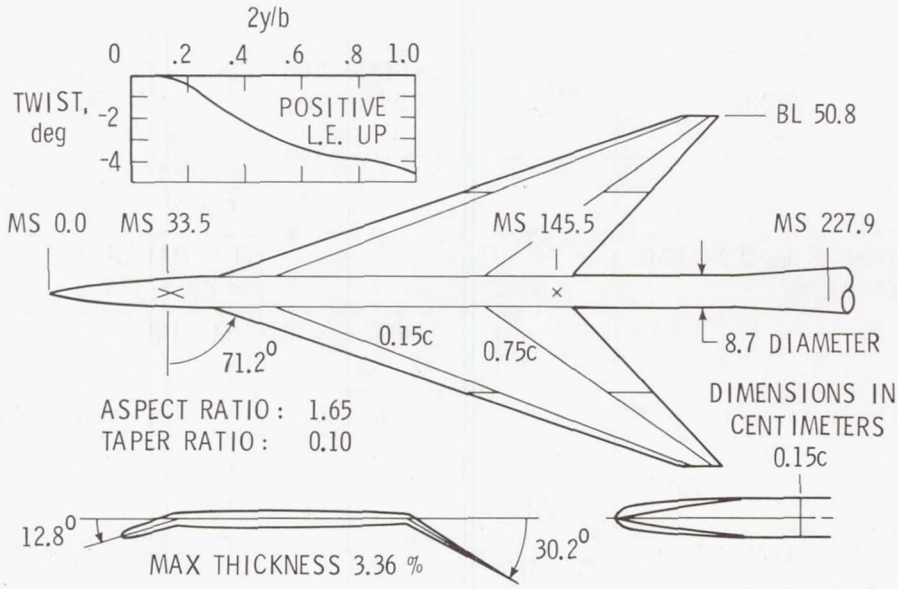

Figure 1.- General arrangement and characteristics of arrow-wing wind-tunnel-model configuration.

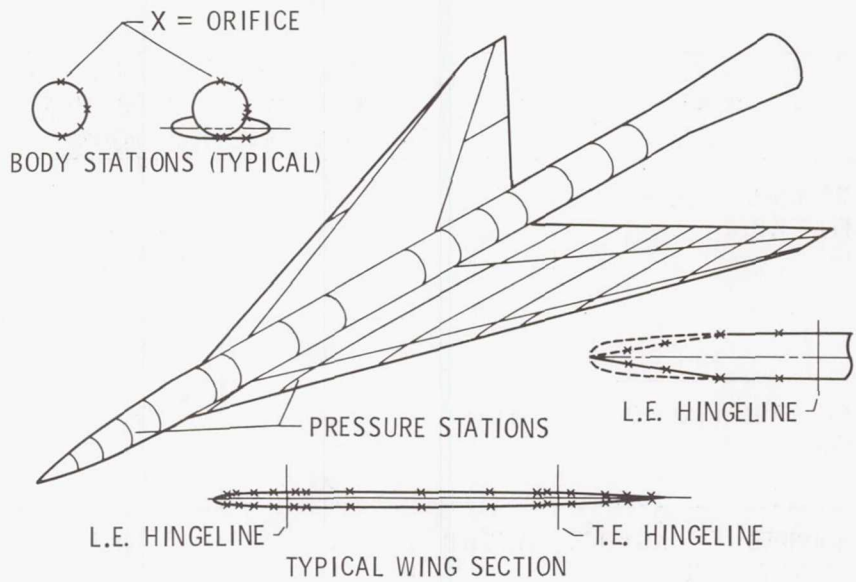

Figure 2.- Pressure orifice locations on wind-tunnel model.

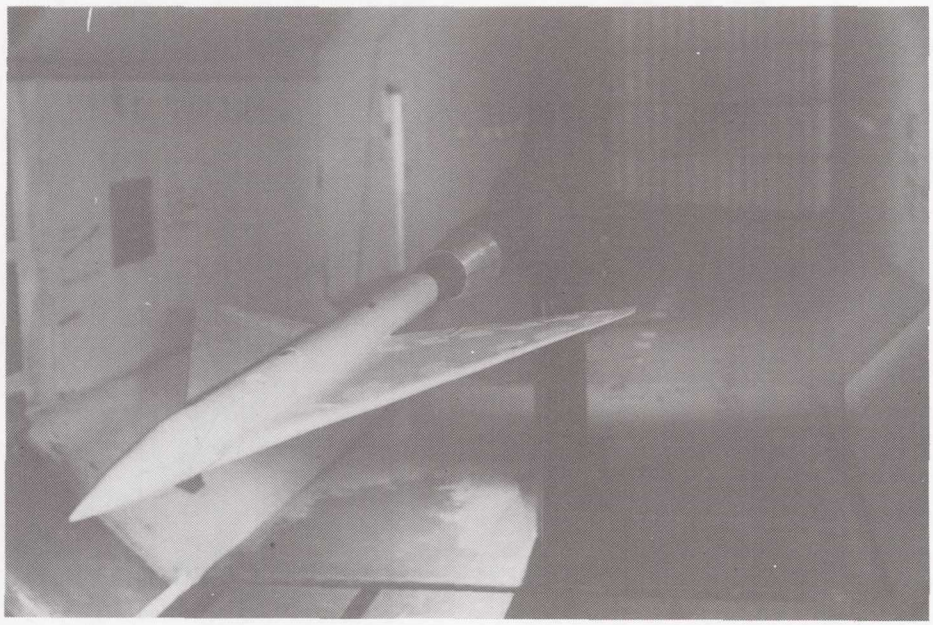

Figure 3.- Flat arrow-wing model mounted in Boeing 8 × 12 ft Transonic Wind Tunnel.

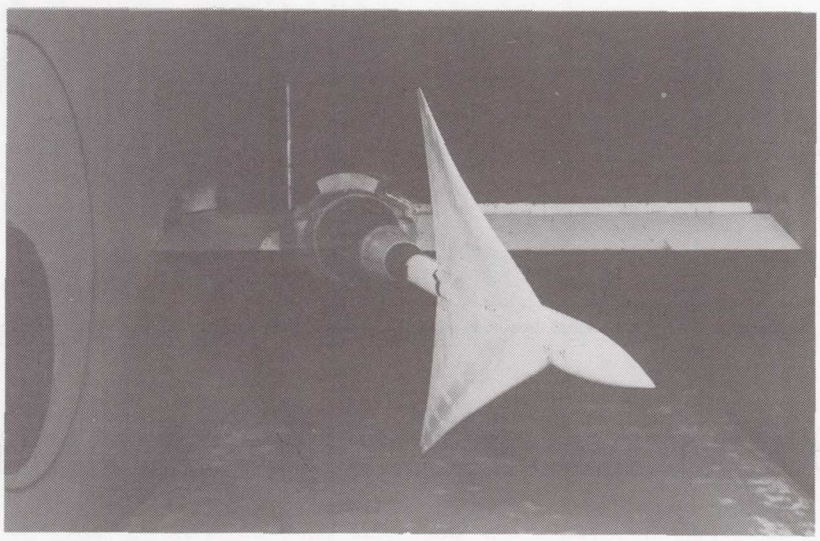

Figure 4.- Twisted arrow-wing model mounted in Ames 9 × 7 ft Unitary Wind Tunnel.

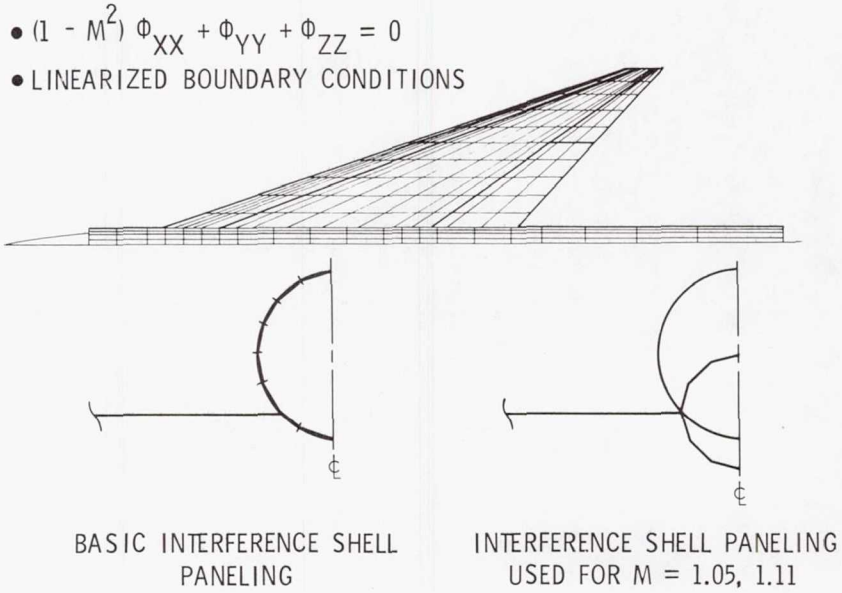

Figure 5.- FLEXSTAB paneling scheme for present arrow wing.

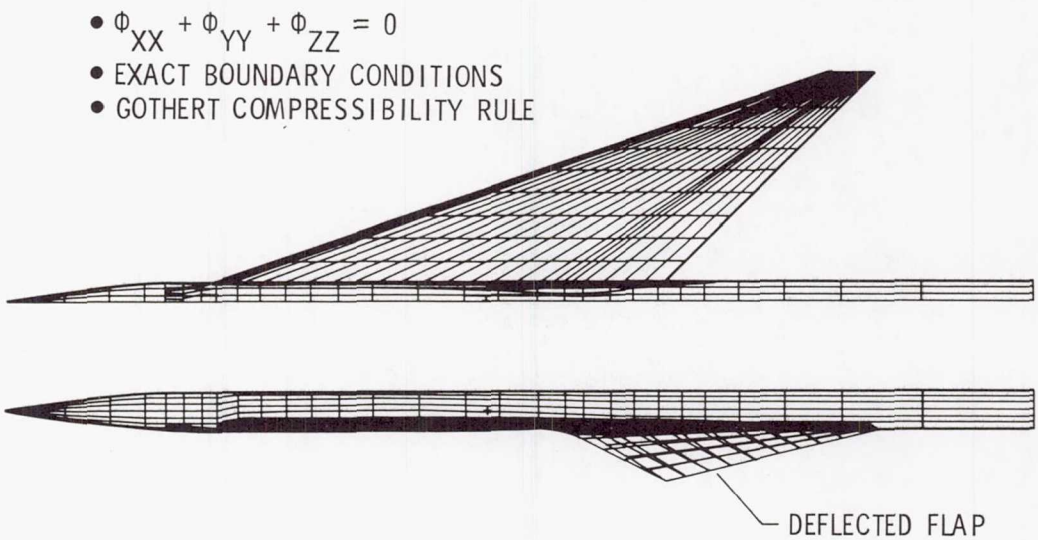

Figure 6.- TEA-230 paneling scheme for present arrow wing.

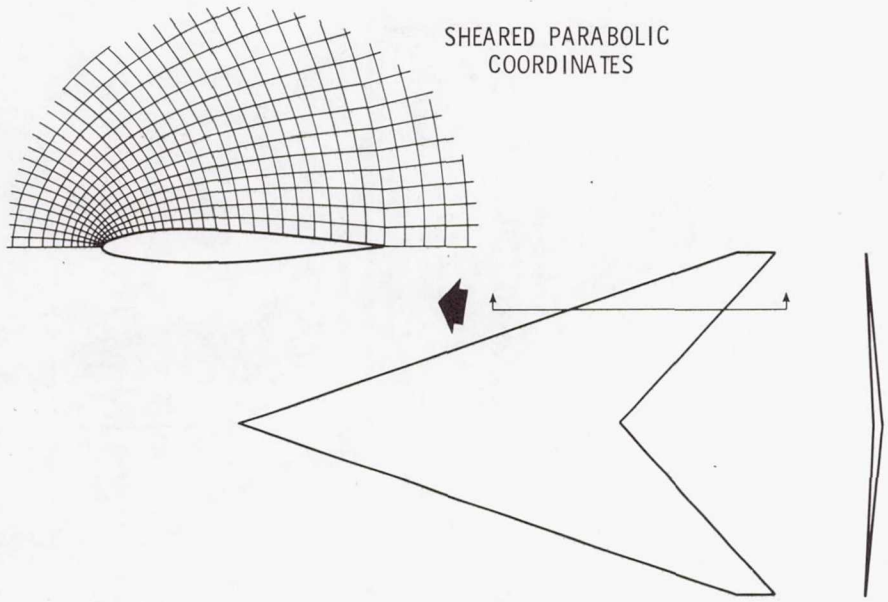

Figure 7.- Sketch showing coordinate scheme used in Jameson-Caughey full-potential-equation numerical method.

- POTENTIAL LIFT DISTRIBUTION - FLEXSTAB
- SUCTION FORCE CALCULATED FROM PRESSURE DISTRIBUTION
- VORTEX LIFT OBTAINED BY ROTATING LEADING EDGE-SUCTION FORCE

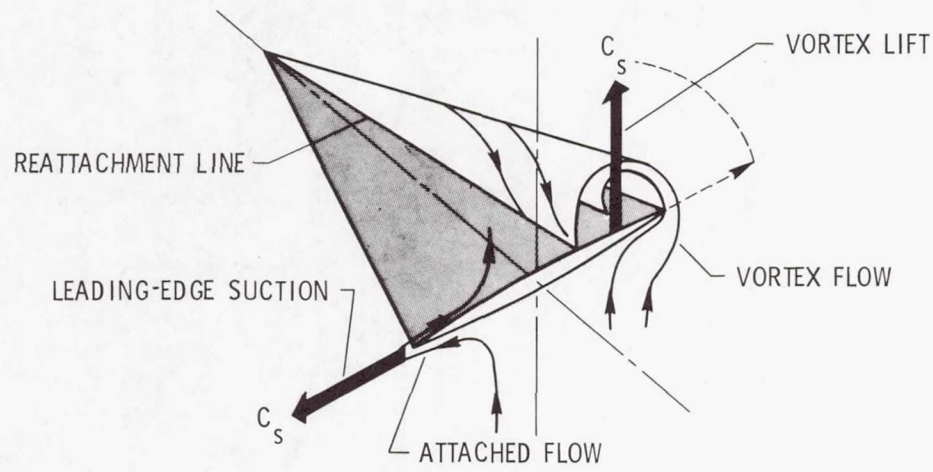

Figure 8.- Basic features of leading-edge suction analogy.

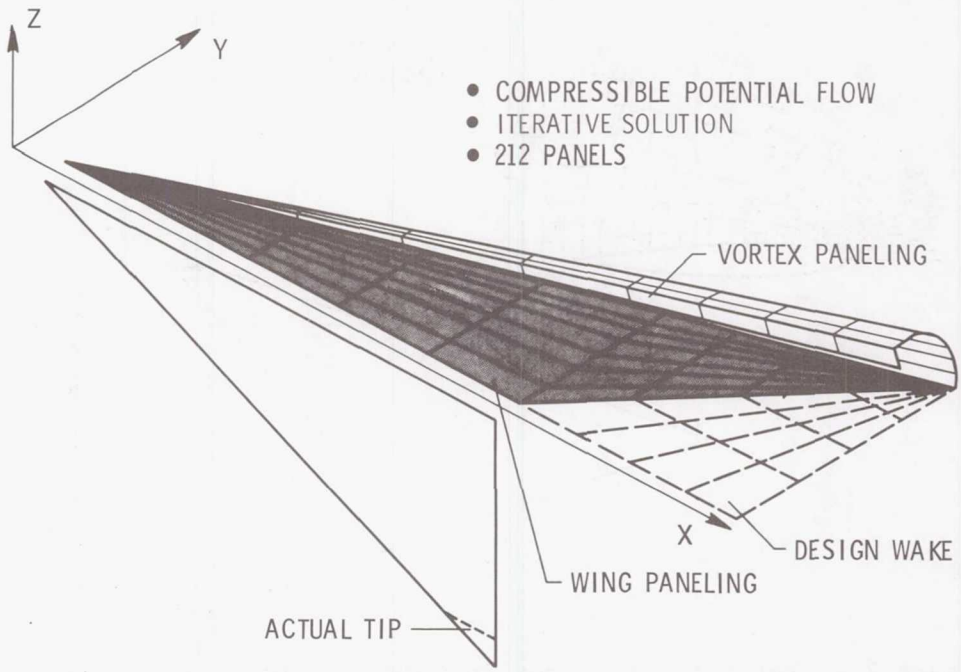

Figure 9.- Three-dimensional vortex program paneling scheme.

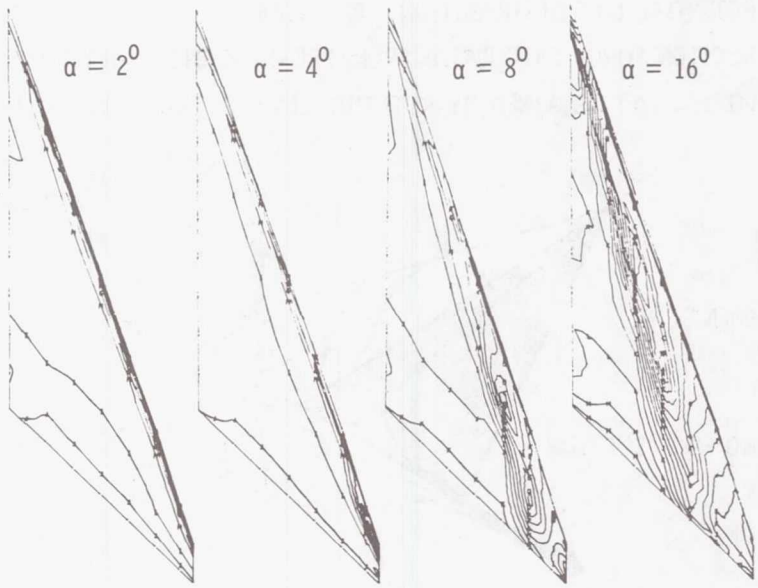

Figure 10.- Upper-surface isobars on rounded-leading-edge flat wing. M = 0.40.

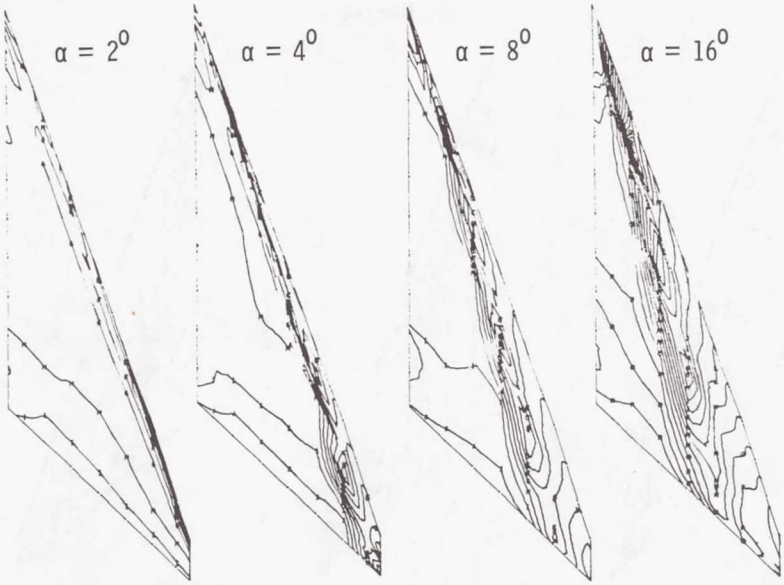

Figure 11.- Upper-surface isobars on sharp-leading-edge flat wing.
M = 0.40.

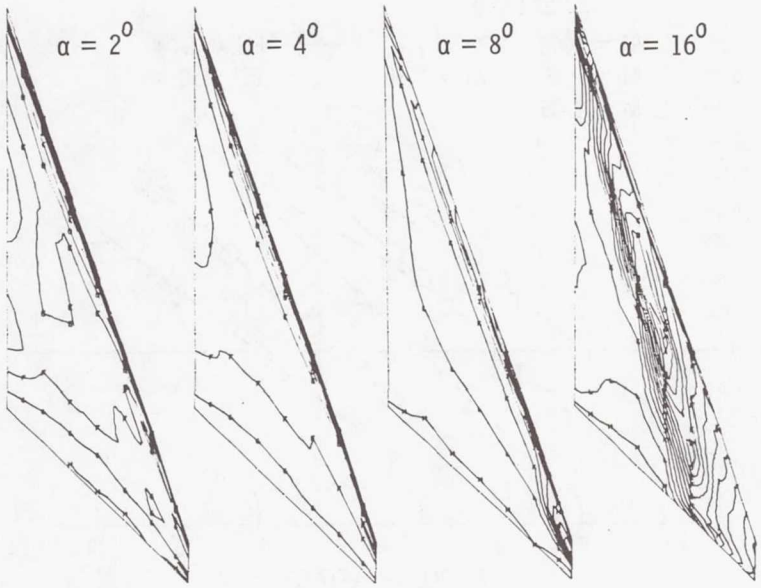

Figure 12.- Upper-surface isobars on rounded-leading-edge twisted wing.
M = 0.40.

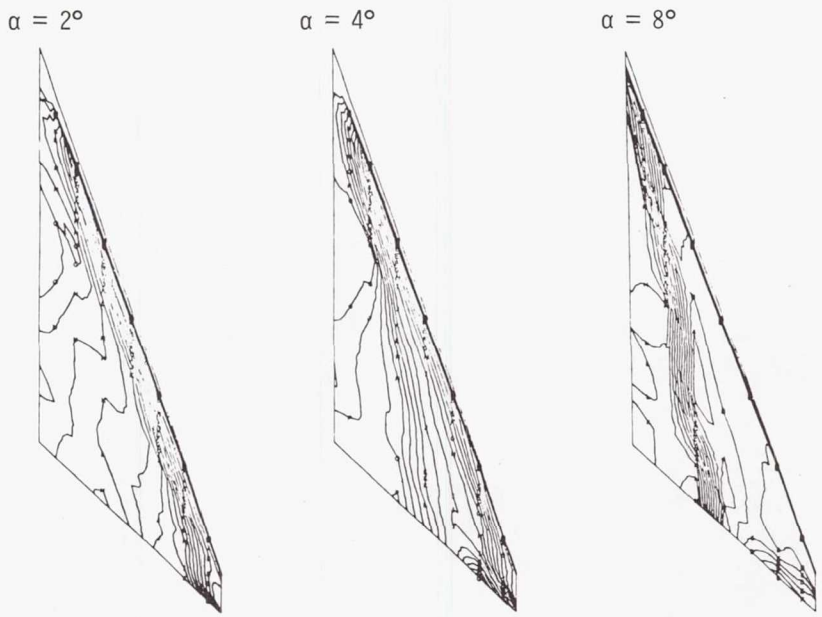

Figure 13.- Upper-surface isobars on rounded-leading-edge flat wing. M = 2.50.

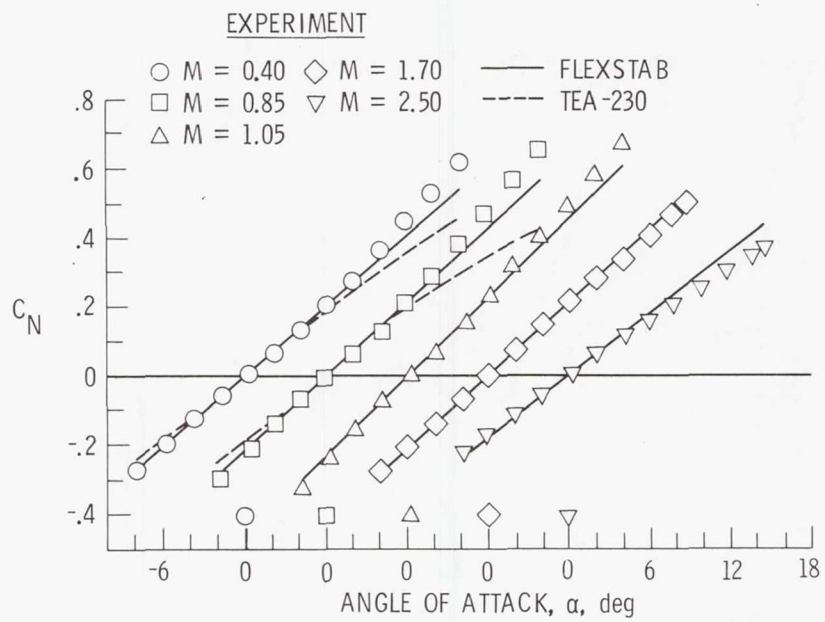

Figure 14.- Total normal force coefficient as a function of angle of attack for flat wing.

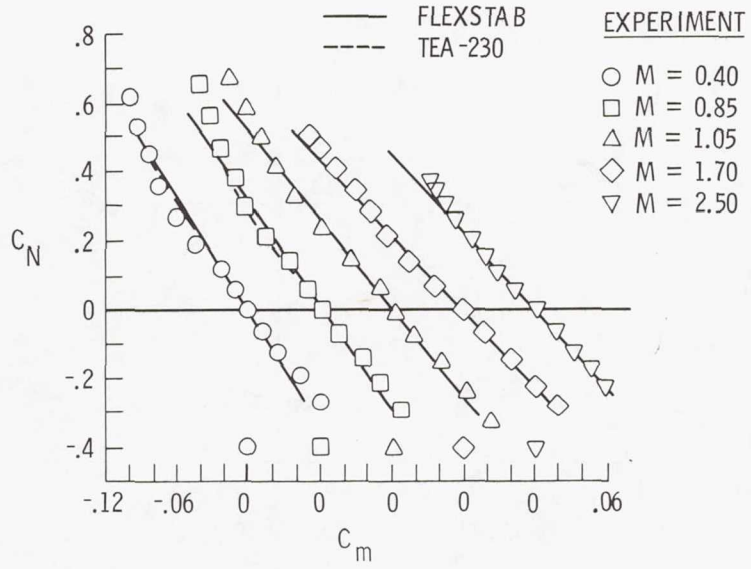

Figure 15.- Total normal force as a function of pitching moment coefficients for flat wing.

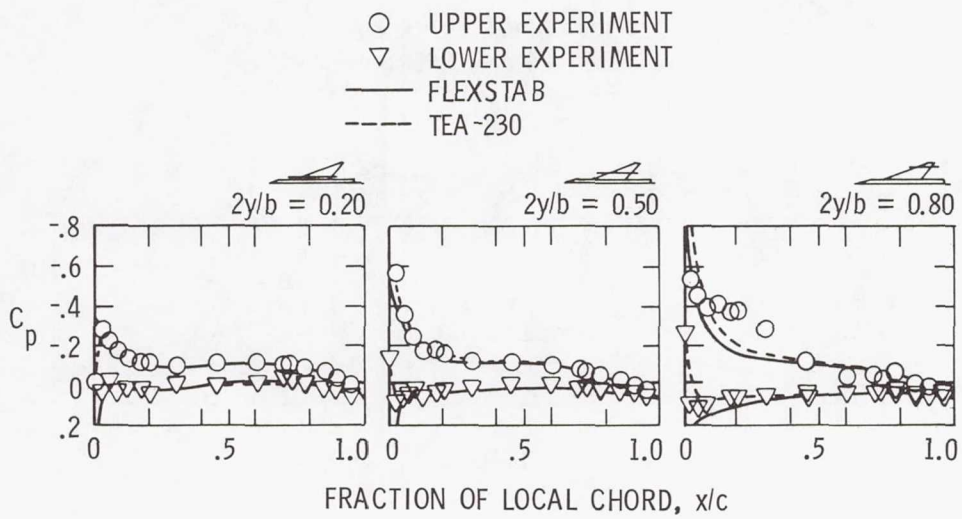

Figure 16.- Surface pressure distributions at three spanwise locations on flat wing. M = 0.85; $\alpha = 4^{o}$.

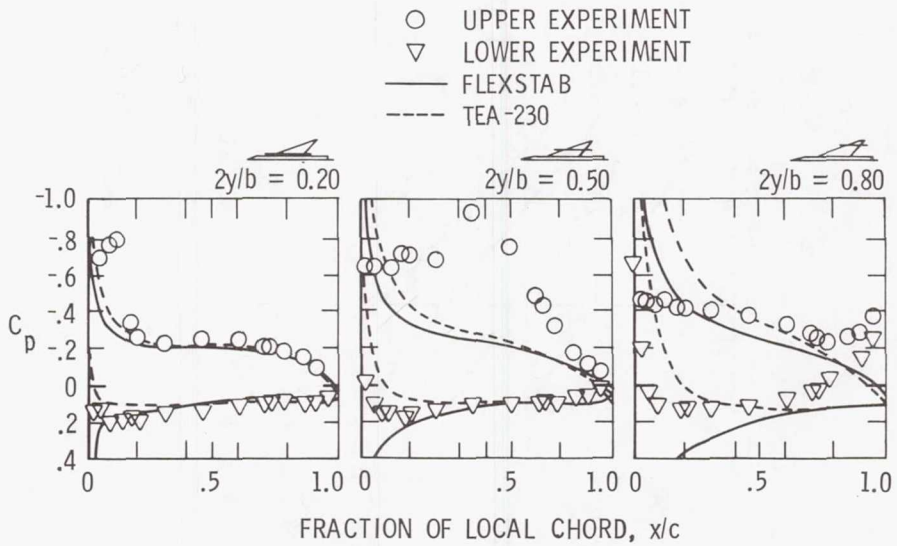

Figure 17.- Surface pressure distributions at three spanwise locations on flat wing. M = 0.85; $\alpha = 12^{o}$.

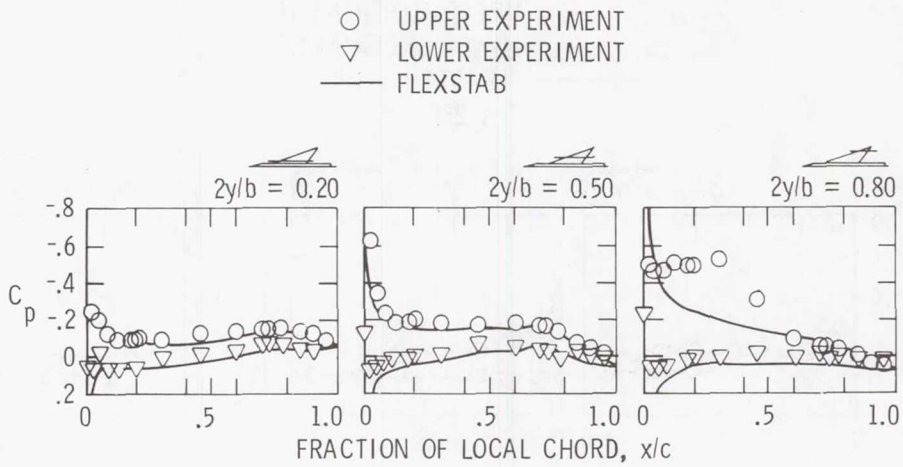

Figure 18.- Surface pressure distributions at three spanwise locations on flat wing. M = 1.05; $\alpha = 4^{o}$.

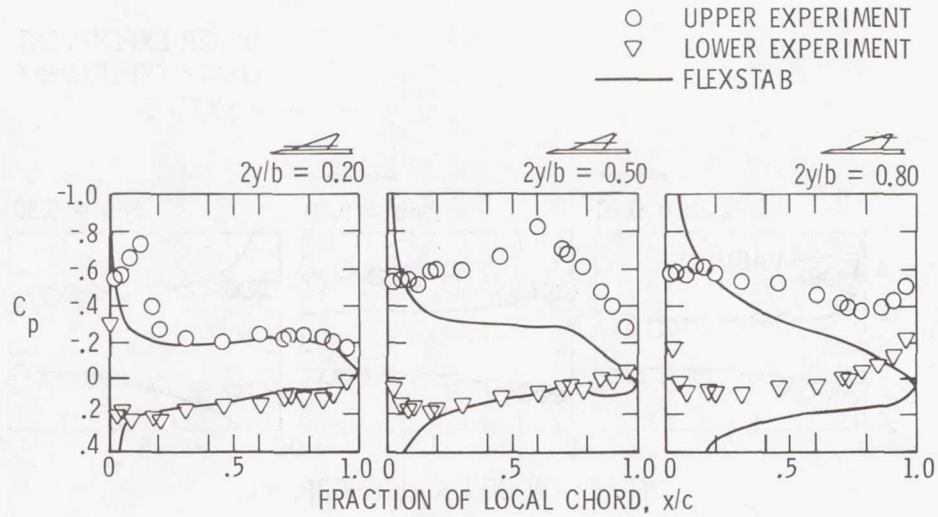

Figure 19.- Surface pressure distributions at three spanwise locations on flat wing. M = 1.05; $\alpha = 12^{\circ}$.

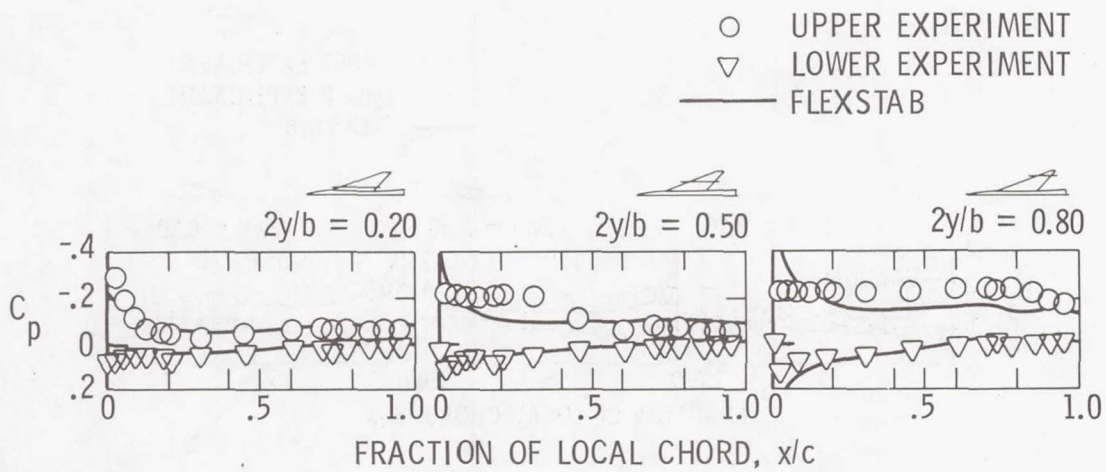

Figure 20.- Surface pressure distributions at three spanwise locations on flat wing. M = 1.70; $\alpha = 4^{\circ}$.

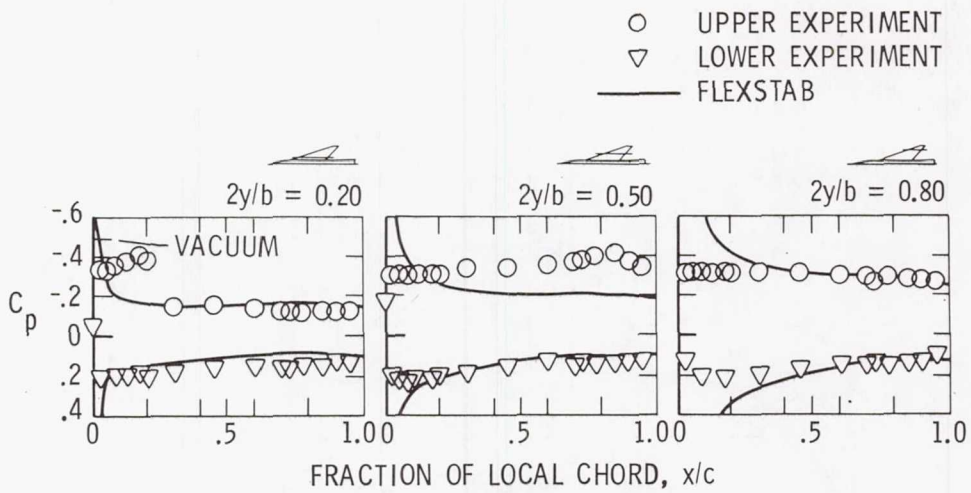

Figure 21.- Surface pressure distributions at three spanwise locations on flat wing. $M = 1.70$; $\alpha = 12^{o}$.

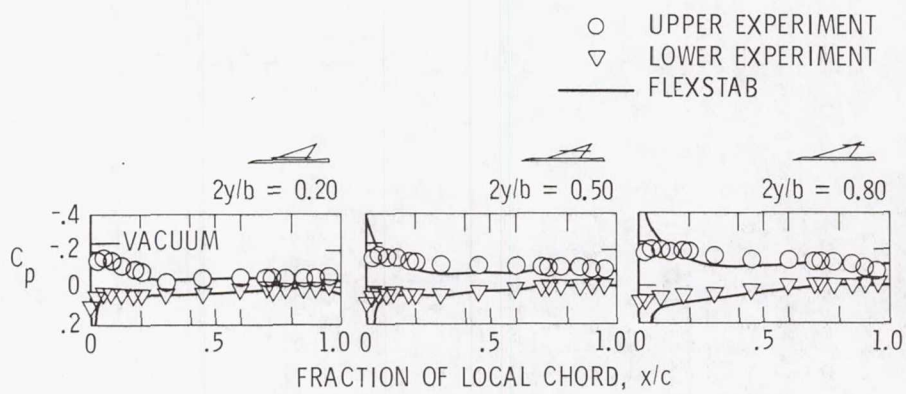

Figure 22.- Surface pressure distributions at three spanwise locations on flat wing. $M = 2.50$; $\alpha = 4^{o}$.

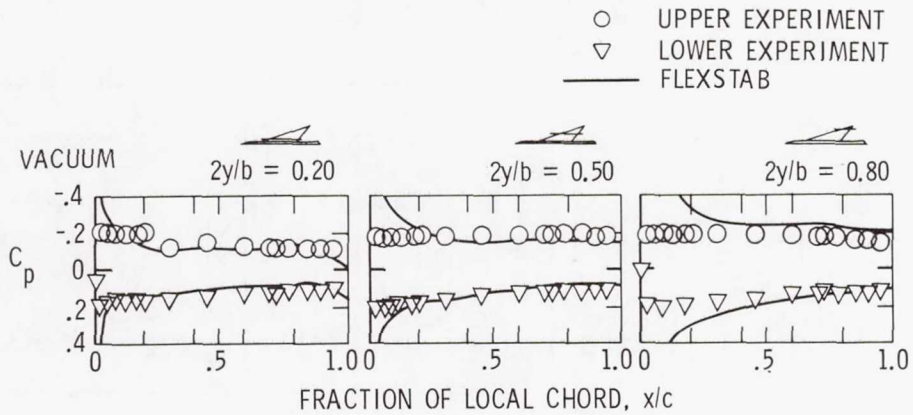

Figure 23.- Surface pressure distribution at three spanwise locations on flat wing. M = 2.50; $\alpha = 12^{o}$.

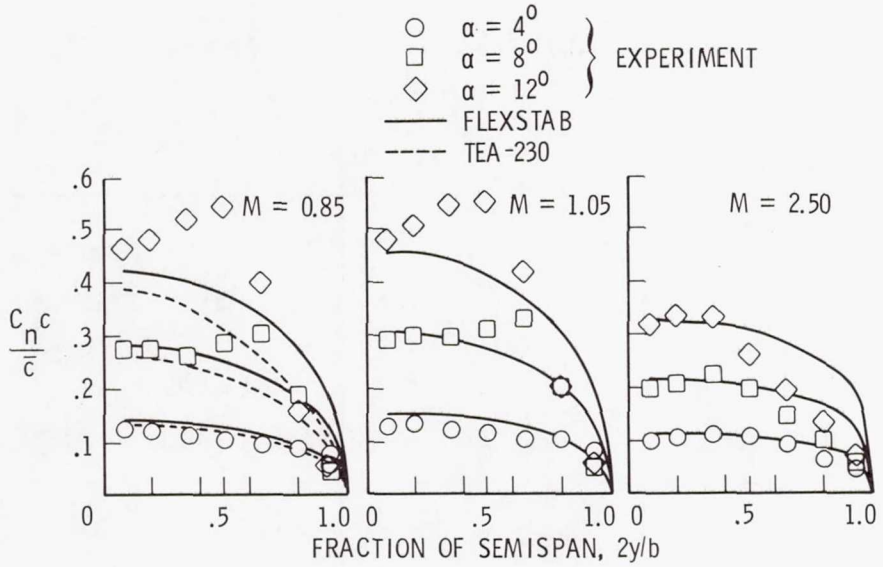

Figure 24.- Spanwise load distributions on flat wing at three Mach numbers and three angles of attack.

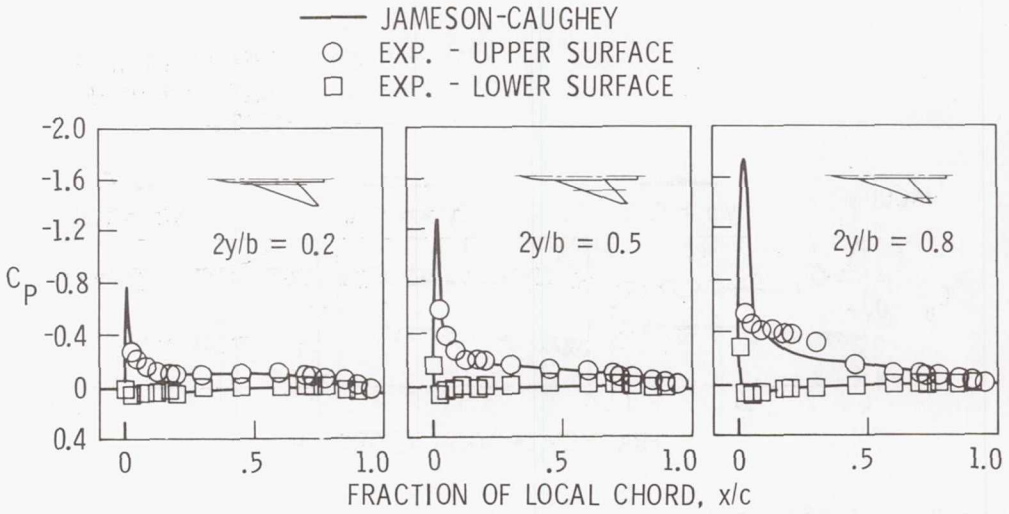

Figure 25.- Comparison of experiment with Jameson-Caughey transonic method. Flat wing; M = 0.85; $\alpha = 4^{o}$.

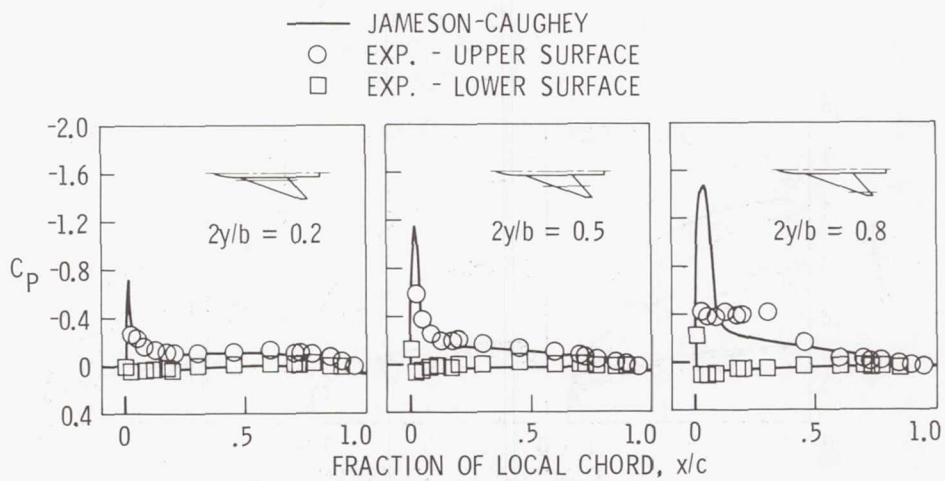

Figure 26.- Comparison of experiment with Jameson-Caughey transonic method. Flat wing; M = 0.95; $\alpha = 4^{o}$.

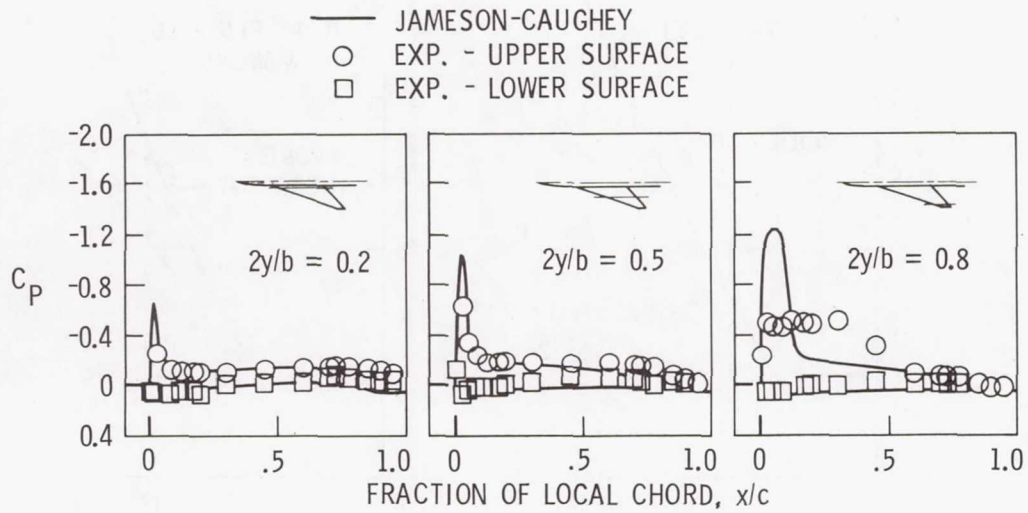

Figure 27.- Comparison of experiment with Jameson-Caughey transonic method. Flat wing; M = 1.05; $\alpha = 4^{\circ}$.

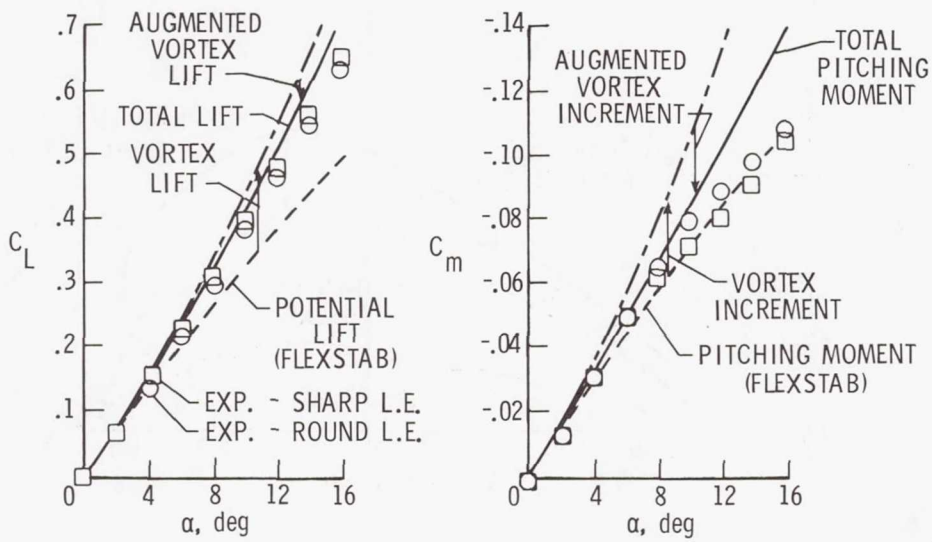

Figure 28.- Comparison of experiment with leading edge suction calculations of lift and pitching moment for flat wing. M = 0.85.

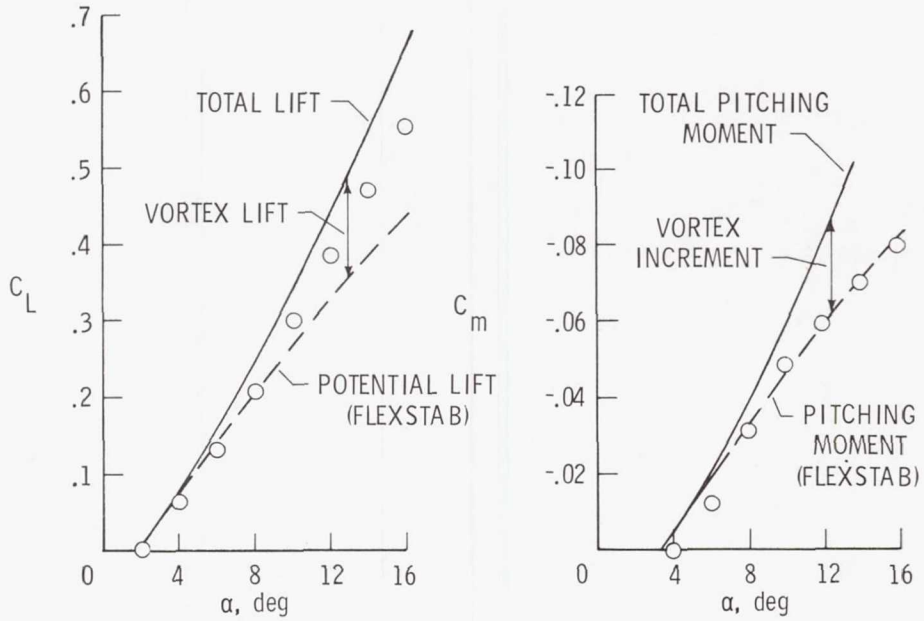

Figure 29.- Comparison of experiment with leading edge suction calculations of lift and pitching moment for twisted wing. M = 0.85.

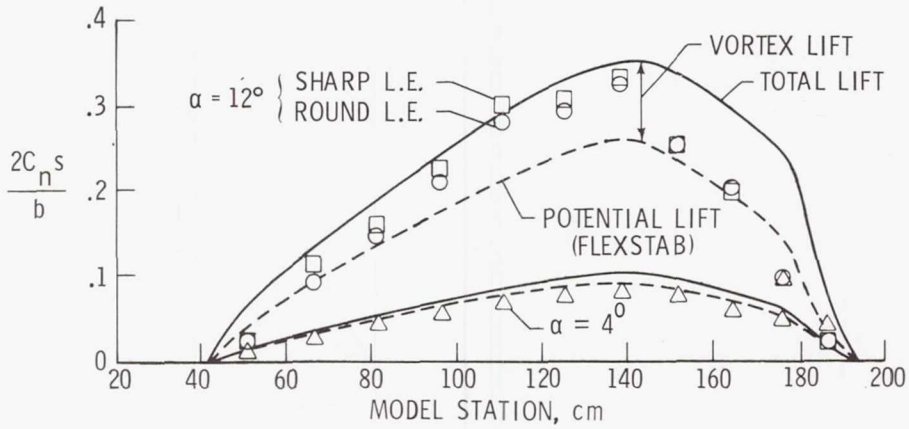

Figure 30.- Comparison of experiment with leading edge suction calculations of longitudinal load distribution for flat wing. M = 0.85.

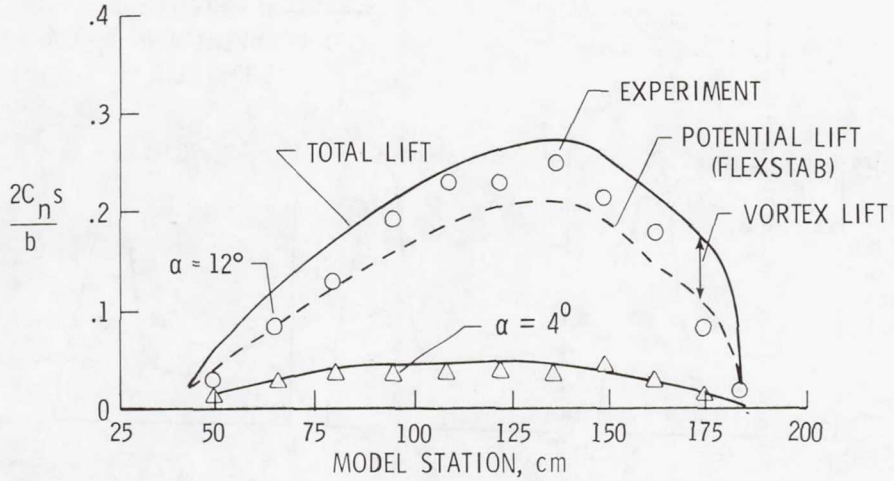

Figure 31.- Comparison of experiment with leading edge suction calculations of longitudinal load distribution for twisted wing. M = 0.85.

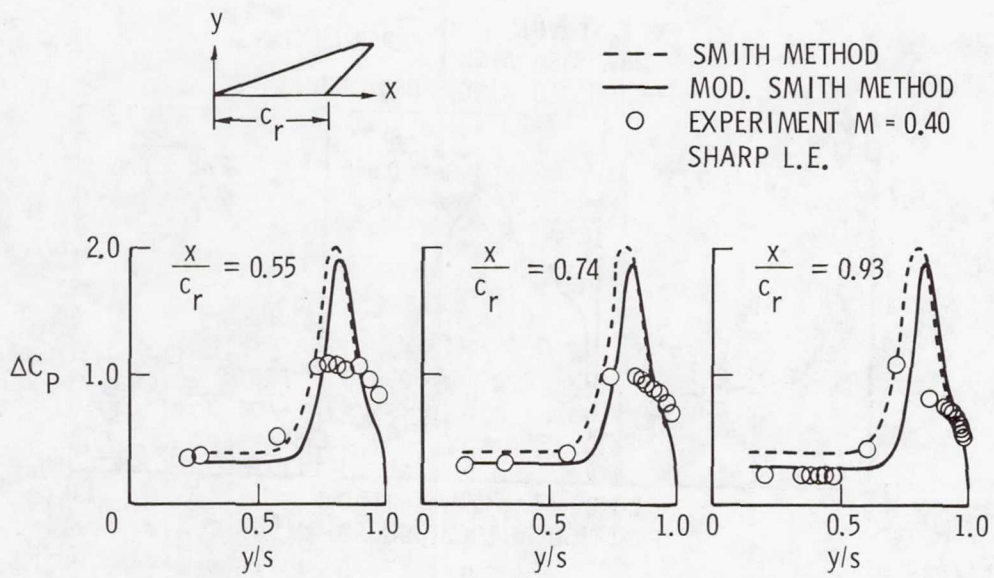

Figure 32.- Theory/experiment comparison of spanwise pressure distributions. Smith and modified Smith methods; α = 12°.

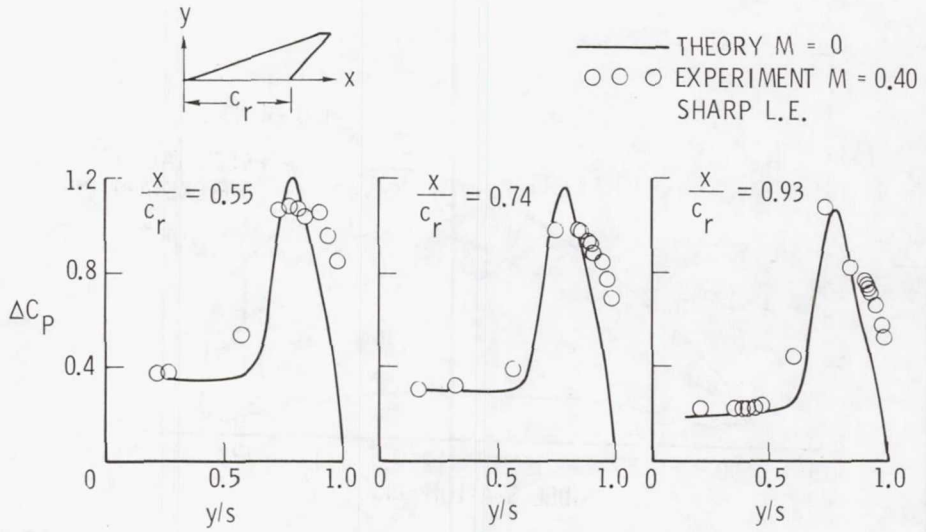

Figure 33.- Theory/experiment comparison of spanwise pressure distributions. Separated-flow panel method; $\alpha = 12^{o}$.

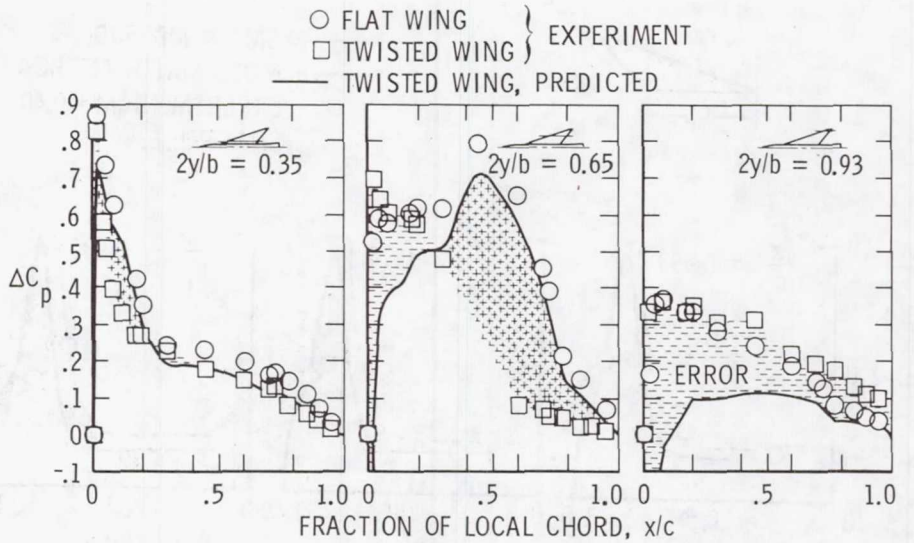

Figure 34.- Pseudo-aeroelastic predictions using linear FLEXSTAB program. M = 0.85; $\alpha = 8^{o}$.

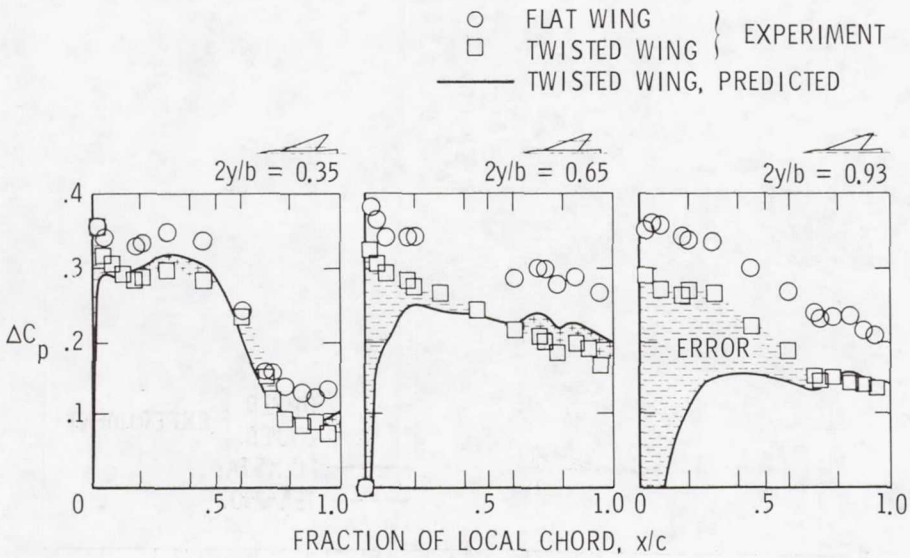

Figure 35.- Psuedo-aeroelastic predictions using linear FLEXSTAB program. M = 2.10; $\alpha = 8^{o}$.

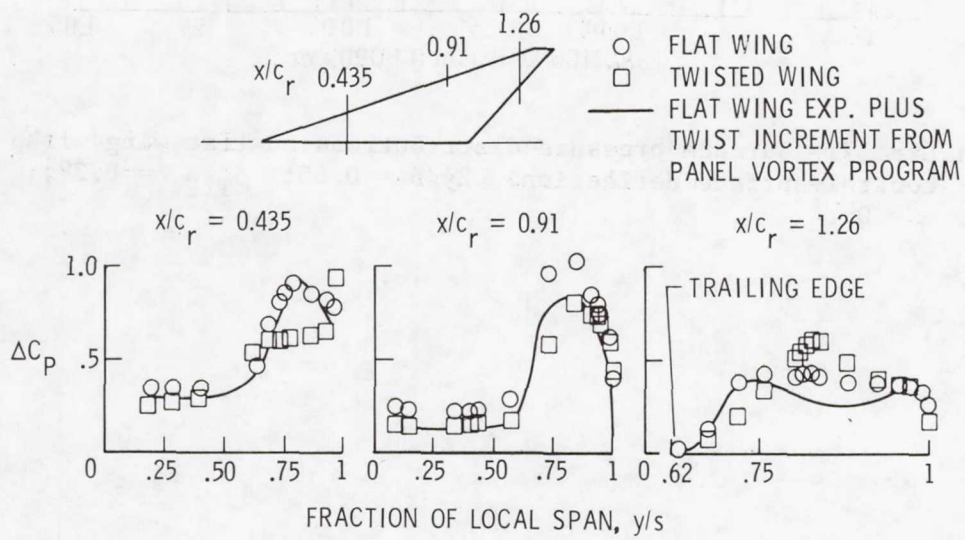

Figure 36.- Pseudo-aerolastic prediction using separated-flow panel program. M = 0.40; $\alpha = 12^{o}$.

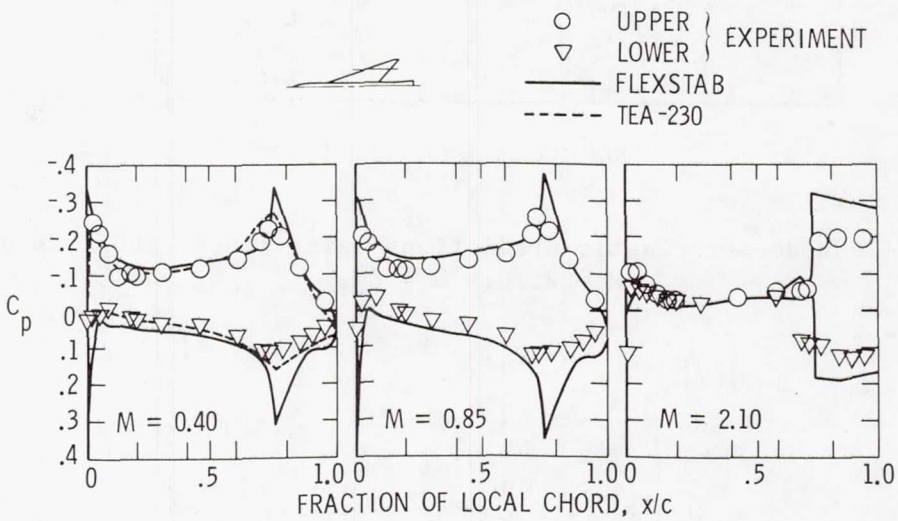

Figure 37.- Surface pressure distributions on flat wing with control-surface deflection. $2y/b = 0.65$; $\delta_{T.E.} = 8.3^{o}$; $\alpha = 0^{o}$.